A torque estimator for a traveling wave ultrasonic motor - application to an active claw

Frédéric Giraud, Betty Semail

▶ To cite this version:

HAL Id: hal-01110739

https://hal.archives-ouvertes.fr/hal-01110739

Submitted on 28 Jan 2015

A Torque Estimator for a Travelling Wave Ultrasonic Motor - Application to an Active Claw

Frédéric Giraud, Betty Semail *Member IEEE*

Abstract - Depending on its electrical to mechanical energy conversion process, the torque on a Travelling Wave Ultrasonic Motor(TWUM)'s shaft is not directly proportional to a measurable electrical variable, such as current or voltage, but is derived from a complicated process at the stator/rotor interface. The load torque is thus quite unknown, and this can be a disadvantage in applications where a torque limitation is required or a torque measurement is needed. The aim of this article is to come up with a straightforward torque estimator on a TWUM. For that purpose, the motor is modelled, this modelling leads to different estimator strategies. More specifically, we chose a strategy for which a speed sensor is useless, relying only on the stator's resonant behavior. The parameters of the motor needed for the estimator are measured afterwards while some non linearities are identified and taken into account. Several experimental trials are then carried out to check the performance of the estimator. Finally, a claw actuated by a TWUM is presented, because this is a typical application where the knowledge of the torque helps guarantee the safety of the device.

I. INTRODUCTION

Travelling wave Ultrasonic Motors (*TWUM*) exploits a piezoelectrically generated flexural wave which propagates at the surface of a stator. This wave is able to propel by contact a rotor strongly pressed on the stator. The friction caused by the contact mechanism provides us with numerous advantages, including: breaking without supply, a high torque to mass ratio and high torque/low speed characteristics. Thus, while a speed reducer is often needed with an electromagnetic motor, it becomes useless in applications using *TWUM* , therefore leading to lightweight and compact applications.

Unfortunately, unlike classical electromagnetic motors, it is very difficult to exactly obtain the torque operating on a *TWUM* shaft. This is due to the different energy conversions and more specifically to the complications caused by the contact mechanism between the stator and the rotor. However, for many applications, limiting or controlling the actuator's torque is necessary; in fact, when a fault appears in a system, the torque on the motor's shaft increases (or decreases) dramatically, which should be detected by the controller. While this can be easily done with a DC-motor, *TWUM* doesn't offer this simplicity naturally.

A torque estimator for a *TWUM* is nonetheless possible to achieve. For instance, in [1], a possible method is proposed: a neural network learns *off line* all the torque-speed characteristics of the motor, while during operation, the torque is estimated *on line* by inverting the network. This method is based on the characterization of the stator/rotor contact mechanism; a speed measurement is necessary and a large number of trials have to be carried out because torque-speed characteristics are not linear.

In this article, a different torque estimator is proposed. This estimator doesn't rely on the mechanical load characteristics, nor on the stator/rotor contact mechanism, but on the stator parameters. This estimator relies on a modeling which is described in the first section of this paper. Then, the torque estimator's principle is then developed as well as an experimental approach which is useful when

identifing the modelling parameters. Finally, the accuracy of the torque estimator is checked on an active claw application, comparing the estimated torque to the measured one.

II. PRINCIPLE OF THE TORQUE ESTIMATOR

A. Modeling overview

Travelling wave ultrasonic motors are often described using an electromagnetic equivalent circuit. The resonant behavior is taken into account by a R-L-C serial branch, while the rotational effect of a mechanical load attached to the motor is modeled by an equivalent parallel resistor [2] [3]; sometimes, the value of the capacitance of the R-L-C branch varies in order to take into account the effect of the axial force which presses the stator against the rotor. This modeling is very useful in designing the power electronics *in front of* the motor, but is not satisfactory when describing the energy conversion process; in fact, this modeling is valid for steady state operations only, and both the normal and tangential forces are mixed in the circuit.

The next section deals with a modeling we proposed for taking into account transitory operations [3][4]. This modelling relies on a two stages decomposition of the stator-rotor contact mechanism. The first stage, named interaction between stator and an "ideal" rotor relies on the assumption of a punctual contact. Punctual means that the stator is in contact with the ideal rotor at one point only along a wavelength. Moreover, no sliding is considered between the ideal rotor and the stator, so both have the same instantaneous speed. The second stage, named interaction between the real and the "ideal" rotor aims at taking into account in a global approach the real contact mechanism so as to fit the experimental torque-speed characteristics. Although the real contact mechanism isn't well described, this modelling has the advantage to lead to simple equations of which the validity domain will be checked in chapter III through experimental trials.

On the figure 1, we have represented the travelling wave which propels the ideal rotor by only one point along a wavelength. In the fame fixed to the contact point $(\overrightarrow{u}_r, \overrightarrow{u}_\theta, \overrightarrow{u}_z)$ the travelling wave propagates toward the right (along $\overrightarrow{u}_\theta$) although the ideal rotor moves toward the left (along $-\overrightarrow{u}_\theta$). We also define the z-axis about which the motor and the contact point turn. The location of the contact point is defined by the rotation angle θ_c, measured from a fixed frame (O, x, y).

1) Causal modeling in (α, β) frame: The *TWUM* is composed of a ring shaped stator on which small piezo-electric elements are bonded. These elements have alternate polling directions, and are divided into two groups, named phase α and phase β. These two phases are supplied by two independent voltages, v_α and v_β. Because of the piezo-electric effect, the **first energy conversion** stage converts these voltages into the forces F_α and F_β inside the stator with:

$$F_\alpha = Nv_\alpha \quad F_\beta = Nv_\beta \tag{1}$$

and N the force factor.

These forces bend the stator. And if the excitation frequency of the two supply voltages is sufficiently close to the resonant frequency of the stator, two stationary waves appear at the stator surface: the
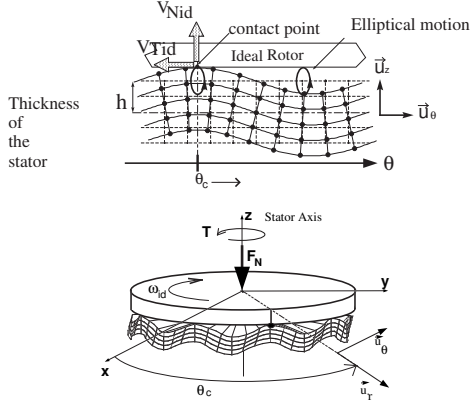
Fig. 1. View of the stator; under punctual contact assumption, the rotor is propelled by one point only along a wavelength.

bending waves, whose height are named w_α and w_β. This **second stage** of the energy conversion can be described by the equation (2)

$$m\ddot{w}_\alpha + d_s\dot{w}_\alpha + cw_\alpha = F_\alpha - F_{r\alpha}$$
$$m\ddot{w}_\beta + d_s\dot{w}_\beta + cw_\beta = F_\beta - F_{r\beta} \quad (2)$$

with

- m the vibrating mass of the stator,
- c the vibrating stiffness of the stator,
- d_s the damping coefficient.

In this equation, $F_{r\alpha}$ and $F_{r\beta}$ have been added to take into account the effect of external forces on the wave propagation. Their expression which depends on F_N (the force pressing the rotor against the stator along the axis of the motor) and F_T' (the tangential force deriving from the load torque T) is quite difficult to determine, and strongly depends on the contact condition at the stator-rotor interface [5][6]. However, in the ideal case of a punctual contact condition, these forces are simply expressed using the location of the contact point θ_c, and the well known rotational matrix, usually used in the study of electromagnetic machines. This calculation has been developed in [4], and derives from power balance of the system:

$$\begin{pmatrix} F_{r\alpha} \\ F_{r\beta} \end{pmatrix} = R(k\theta_c) \begin{pmatrix} F_N \\ F_T' \end{pmatrix} \quad R(\theta) = \begin{pmatrix} \cos(\theta) & -\sin(\theta) \\ \sin(\theta) & \cos(\theta) \end{pmatrix} \quad (3)$$

with

$$F_T' = k\frac{h}{b^2}T \quad (4)$$

And

- h the thickness of the stator
- b the radius of the rotor
- $k = \frac{2\pi b}{\lambda}$ with λ the wavelength of the excited mode.

The contact points are located at the travelling wave's crest. It can be shown that they are situated at an angle given by w_α and w_β using the expression shown in (5)

$$k\theta_c = atan\left(\frac{w_\beta}{w_\alpha}\right) \quad (5)$$

This can be summarized by figure 2; in this figure, we define **W**, a time varying vector, which co-ordinates are w_α and w_β. And in the same way, v_α and v_β are projections of a time varying vector **V** on axis α and β. In this figure, a (d,q) frame appears, but will be explained further.

Moreover, as it can be seen in figure (1), the contact point speed which propels the rotor, has two components:
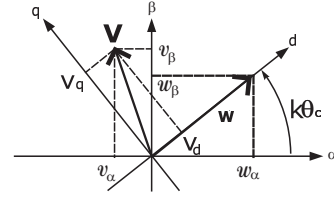

Fig. 2. Voltage vector **V** and Wave vector **W** in (α, β) frame.

- V_{Nid} along the axis of the motor, lifts up the rotor to enable the propagation of the travelling wave. During steady state, this speed is null.
- V_{Tid}' in the tangential direction, from which the rotational speed of the rotor ω_{id} derives.

A kinetic study of the vibrating stator shows then that the expression of those speeds can be written using $\dot{w}_{\alpha\beta}$ and $R(k\theta_c)$ once again:

$$\begin{pmatrix} V_{Nid} \\ V_{Tid}' \end{pmatrix} = R(-k\theta_c) \begin{pmatrix} \dot{w}_\beta \\ \dot{w}_\alpha \end{pmatrix} \quad (6)$$

The rotational speed of the ideal rotor ω_{id} and V_{Tid}' is given by equation (7)[2]:

$$\omega_{id} = k\frac{h}{b^2}V_{Tid}' \quad (7)$$

However, the speed ω_{id} does not actually correspond to the rotor speed, because the contact conditions observed at the stator-rotor interface are very different from those of the ideal contact conditions: in fact, because of friction, the actual rotational speed ω of the rotor decreases with the load torque T. Several models ([6][7][8]) exist to describe this behavior, but they are too complex to be taken into account in a control scheme. In order to achieve a straightforward modelling which may be useful for actuator control, a linear modelling for the global behavior of the motor can be proposed based on experimental results. This is **the third energy conversion**, given by equation (8) and (9).

$$T = f_0 \left(\omega_{id} - \omega\right) \quad (8)$$

$$F_N = K_N \int \left(V_{Nid} - V_N\right) \quad (9)$$

Of course, this process is very non linear, and the value of the parameters f_0 and K_N should vary as a function of the operating point. However, we find here the key variables governing the evolution of the motor torque: the amplitude of the travelling wave, because ω_{id} derives using it, and the rotational speed of the rotor itself. This roughly outlines the torque estimator described in [9] from the speed and the stator's deformation measurements.

In addition, the dynamic of the rotor, along the two degrees of freedom, leads to lay down two other equations:

$$m_r \frac{dV_{Nid}}{dt} = F_N - F_\tau \quad (10)$$

$$J_r \frac{d\omega}{dt} = T - T_r \quad (11)$$

Where:

- m_r and J_r are respectively the mass and rotational inertia of the rotor,
- T_r is the external load torque applied on the rotor,
- F_τ is the normal force pressing the rotor against the stator.

Finally, all these equations yield a modeling which can be represented by way of a Causal Ordering Graph as shown in figure 3. In this diagram we see the internal variables of the system, the ellipses

represent the equations using integral relations (single arrow) or independent time relations (double arrow) only. The relations named R_x are refereed to the equation number (x) in the paper. This method is helpful in deducing the control scheme all it requires is a simple inversion of the graph.
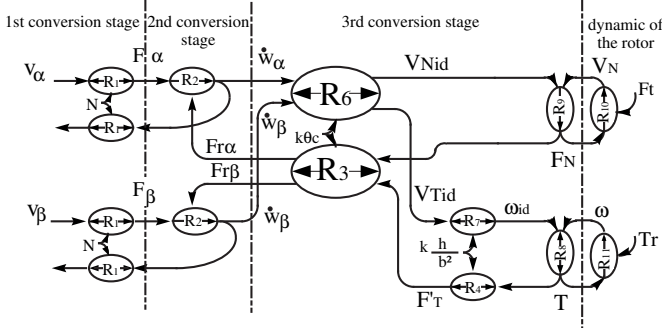

Fig. 3. Causal ordering graph of the *TWUM* .

The graph in figure (3) is divided into four parts, each one represents one energy conversion process or the dynamic of the rotor. Moreover, it shows the couplings of the motors:

- the two independent voltage lines α and β are coupled *via* the rotational matrix,
- the two external forces F_N and F_T' are mixed and $F_{r\alpha}$ and $F_{r\beta}$ act on the travelling wave.

These couplings make global comprehension of the system difficult. This is why in the next section we try to remove them by taking advantage of the experience of the modelling of the electromagnetic AC machines.

2) Causal modelling in a rotating reference frame: the two rotational matrices, on the stationary waves (eq. 6) and on the forces (eq. 3), lead to setting down two new variables V_d and V_q. As it is for the electromagnetic machines where current or voltages are expressed in a rotating reference frame fixed to the rotating electromagnetic field, V_d and V_q represent the supply voltages in a rotating reference frame fixed to the rotating travelling wave. So, this leads us to set down:

$$\begin{pmatrix} v_\alpha \\ v_\beta \end{pmatrix} = R(k\theta_c) \begin{pmatrix} V_d \\ V_q \end{pmatrix} \tag{12}$$

So, according to the figure 2, V_d and V_q are the coordinates of the voltage vector **V** in the rotating frame (d, q). Using V_d and V_q, equations 2, 3, 6, are revised to produce two new equations respectively on d axis and q axis respectively, where the couplings are removed:

$$m\dot{V}_{Nid}' + ds V_{Nid}' + (c - mk(\dot{\theta}_c)^2) \int V_{Nid}' dt = NV_d - F_N' \tag{13}$$

$$2m\dot{V}_{Tid}' + ds V_{Tid}' = NV_q - F_T' \tag{14}$$

In fact, in equation (14), the variables of the tangential axis appear only on the q axis, though equation (13) shows that the normal variables only appear on the d axis. This equation is of second order type, and completely describes the resonant behavior of the motor.

Figure (4) shows the Causal Ordering Graph of the actuator in the rotating reference frame, reduced to the q axis as it deals with the torque.

Thanks to this graph's inversion, it is easy to deduce the torque control of the piezo-actuator [3]; however, in this paper, we focus our attention on the torque estimator, which is what the next section deals with.
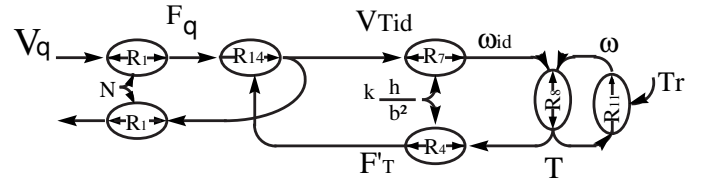

Fig. 4. Causal ordering graph of the TWUM in the rotating reference frame; axis q only.

B. The torque estimator

The principle of a torque estimator is outlined by inverting the Causal ordering graph of the figure 4. There are thus three different paths, as summarized figure 5:

- 1- from relation (11). This is difficult because both the load inertia and the load torque T_r should be known,
- 2- from relation (8) and the measurements of both ω and ω_{id} as proposed by [9]; this estimator needs the identification of the parameter f_0,
- 3- from relation (14) and the measurements of V_q and V_{Tid}'.
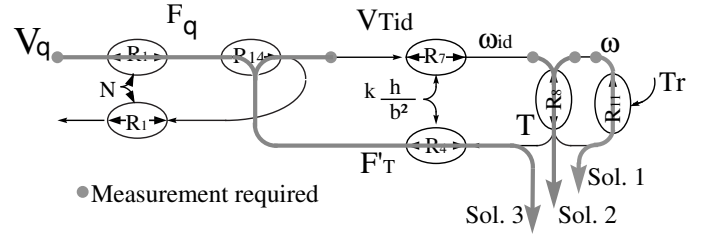

Fig. 5. The three different ways to estimate the torque T can be deduced from the inversion of the COG.

In order to avoid a speed sensor, the torque estimator will rely on equation 14. However, inverting this equation is not straightforward, because of the derivative term $2m\dot{V}_{Tid}'$, which should be approximated. A closed loop estimator could then be proposed, whose output would converge toward the solution. But considering a high performing estimator is required especially in the case of steady state operations – or slow variations of V_{Tid}', the problematic term $2m\dot{V}_{Tid}'$ is deleted in equation (14):

$$ds V_{Tid}' = NV_q - F_T' \tag{15}$$

Finally, using equations 4 in 15 leads to

$$T = \frac{b^2}{kh} \left[NV_q - d_s V_{Tid}' \right] \tag{16}$$

Achieving the torque estimator.

III. EXPERIMENTAL SETUP

A. The experimental test bench

1) Measuring V_q: The TWUM used during the test is a Shinsei USR30 [10]. This motor has a $30mm$ diameter and can provide a rated torque of $0.1Nm$ for a rated speed of $200rev/min$. It is a commercial product and thus is readily available. On the stator of this motor, an extra electrode is glued to the ring of piezo material. Due to the direct piezo-electrical conversion, the voltage measured on this sensor, named v_{EA}, is directly proportional to the deformation of the stator at this point. Unfortunately, this deformation is a combination of w_α and w_β: thus it is difficult to build θ_c from the equation (5)

because w_α and w_β are not measured independently. In that case, measuring V_q from V_α, V_β and (12) is impossible.

This leads us to set down the assumption that the amplitude of the two stationary waves are sinusoidal functions of time in quadrature, so:

$$w_\alpha(t) = W cos(2\pi f t)$$
$$w_\beta(t) = W sin(2\pi f t) \qquad (17)$$

With f the frequency of the supply voltages and W the travelling wave's amplitude.

In order for this assumption to be fulfilled the construction of the must be sufficiently careful as to ensure a good positioning of the stator's electrodes on the piezo ring, thus avoiding dissymmetry between the two phases. However, this condition is often achieved in the Shinsei USR30 when it is supplied by two sinusoidal voltages in quadrature with the same amplitude:

$$v_\alpha(t) = V cos(2\pi f t + \Psi)$$
$$v_\beta(t) = V sin(2\pi f t + \Psi) \qquad (18)$$

with V the amplitude of supply voltages, and Ψ, the phase difference between $v_\alpha(t)$ and $w_\alpha(t)$. On the experimental test bench, V is kept constant, though f varies.

On the one hand, the equations (5) and (17) yield to:

$$\theta_c = atan \frac{W sin(2\pi f t)}{W cos(2\pi f t)}$$
$$= 2\pi f t \qquad (19)$$

On the other hand, if we consider the location of the sensor, v_{EA} is in fact proportional to $K(w_\alpha + w_\beta)$, with K the conversion factor of the auxiliary electrode. This consideration yields to:

$$v_{EA} = K(W sin(2\pi f t) + W cos(2\pi f t))$$
$$= K \frac{\sqrt{2}}{2} W cos(2\pi f t + \frac{\pi}{4}) \qquad (20)$$

In conclusion, from equations (19), (12) and (20), θ_c is equal to the instantaneous phase of the sensor's voltage v_{EA} minus $\frac{\pi}{4}$.

The considerations of equations (19) and (12) yields:

$$\begin{pmatrix} V_d \\ V_q \end{pmatrix} = R(-2\pi f t) \begin{pmatrix} V cos(2\pi f t + \Psi) \\ V sin(2\pi f t + \Psi) \end{pmatrix} = \begin{pmatrix} V cos(\Psi) \\ V sin(\Psi) \end{pmatrix} \qquad (21)$$

So, V_q may be deduced by:

$$V_q = V sin(\Psi) \qquad (22)$$

and Ψ can be measured from the phase difference between v_α and v_{EA}, which is experimentally achieved thanks to an integrated chip.

2) Measuring V'_{Tid}: to complete the identification of T from equation (16), it is necessary to know V'_{Tid}, but however this is an internal variable. It may be calculated thanks to equation (6), and from the measurement of $\dot{w}_\alpha$ and $\dot{w}_\beta$. Once again, to reach these values, we use the previous assumption which leads to equation (17)

$$\dot{w}_\alpha(t) = \dot{W} cos(2\pi f t) + (2\pi f) W sin(2\pi f t)$$
$$\dot{w}_\beta(t) = \dot{W} sin(2\pi f t) + (2\pi f) W cos(2\pi f t) \qquad (23)$$

Of course, in order to obtain the equation (23) we need to consider that the excitation frequency f is kept constant. This is not rigorously correct during transitory operations. But the stator of a TWUM is a mechanical resonator, f is chosen very close to its resonant frequency and thus considered constant.

Using equations (23), (19) and the rotational matrix (6) now yield:

$$V'_{Tid} = -\dot{w}_\alpha sin(2\pi f t) + \dot{w}_\beta cos(2\pi f t)$$
$$= \left(-\dot{W} cos(2\pi f t) + (2\pi f) W sin(2\pi f t) \right) sin(2\pi f t)$$
$$+ \left(\dot{W} sin(2\pi f t) + (2\pi f) W cos(2\pi f t) \right) cos(2\pi f t) \qquad (24)$$
$$= (2\pi f) W (sin^2(2\pi f t) + cos^2(2\pi f t))$$
$$= (2\pi f) W$$

Therefore, V'_{Tid} is proportional to the travelling wave's amplitude. If we now take equation 20 into account, W can be deduced by extracting from v_{EA} its own amplitude named $\hat{V}_{EA}$. V'_{Tid} is given by:

$$V'_{Tid} = (2\pi f) \frac{1}{K \frac{\sqrt{2}}{2}} \hat{V}_{EA} \qquad (25)$$

Since the different state variables of the torque estimator can be measured, the next section deals with the identification of the parameters appearing in the equation 16.

B. Measurement of the stator parameters

Several methods have been proposed to identify stator parameters [11]. Most of them rely on the *electrical equivalent circuit*, and the parameters are found by fitting the curve of the variation in the frequency of the current into a phase with a 2nd order type equation. However, this approach has several drawbacks among which there is the difficulty, firstly of precisely detecting the stator's resonance - because a small variation of the frequency leads to a greater variation of the current when approaching the resonance frequency - and secondly of carrying out an identification of the effect of the tangential forces.

This is why we proposed an other method [4]. This approach relies on a V_q control detailed in [3] which allows easy characterisation of the resonant frequency and avoidance of couplings between the normal and tangential axes. The identification process is divided into two steps:

- identification of d_s

- identification of $k \frac{h}{b^2}$

1) Identification of d_s: For an unloaded motor which has reached its steady state, the travelling wave's amplitude W derives from the equation 16 where T is set to 0. In these conditions:

$$d_s 2\pi f W = N V_q \qquad (26)$$

Due to the experimental test bench, and equation (22), Ψ is in fact tuned instead of V_q, and this equation is transformed into:

$$d_s 2\pi f W = N V sin(\Psi) \qquad (27)$$

Identifying d_s can then be achieved by keeping V constant; plotting the evolution of W against Ψ should result in a sinusoidal shape, whose crest gives the ratio $\frac{N}{d_s 2\pi f}$.

However, this method is quite sensitive to non linearities which induce variations of d_s with W [12]. This is why, instead of V, W is kept constant. So, for each value of Ψ, V is tuned in order to have W equal to a value we fixed before.

A closed loop including a *Voltage Controlled oscillator* controls the voltage frequency f so as to have the required value for Ψ. This angle is measured by using a phase detector (figure 6); the controlled scheme has been previously described in [3].

We then plot the evolution of $\frac{W}{V}$ against Ψ. The experimental trials, for each rotational direction and several wave amplitude, are given in figure 7. Table I summarizes the values of d_s identified from
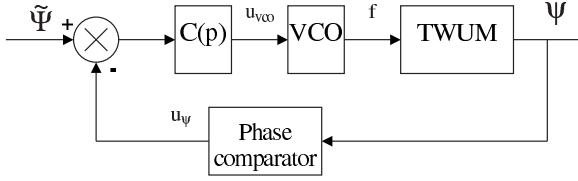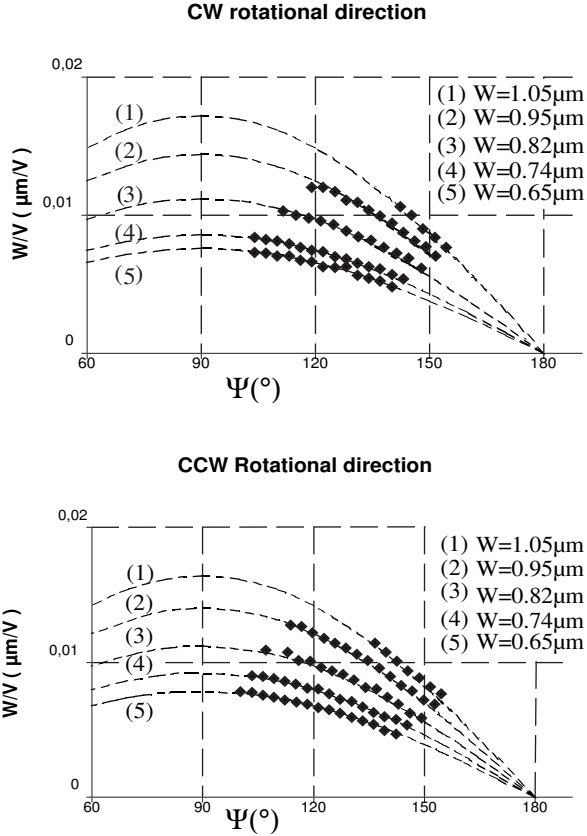
Fig. 6.   Closed loop for the control of Ψ.

Fig. 8.   Evolution of d_s as a function of $\frac{1}{W}$ for both rotational direction and fitting.

$$d_{s0} = 19.2 N.s.m^{-1} \qquad \rho = 47.8.10^{-6} N.s$$

So, taking into account the non-linearity of d_s, the torque estimator can be achieved by merging the equations 16, 23 and 28:

$$(-d_{s0} + \frac{\rho}{W})2\pi fW = NV_q - k\frac{h}{b^2}T$$
$$-d_{s0}2\pi fW + 2\pi f\rho = NV_q - k\frac{h}{b^2}T \qquad (29)$$
$$d_{s0}2\pi fW = 2\pi f\rho + k\frac{h}{b^2}T - NV_q$$

In this equation, the global parameter $k\frac{h}{b^2}$ is still to be calculated. This next section deals with this calculation.

2) Identification of $k\frac{h}{b^2}$: The identification of this parameter derives once again from equation (16). But now, T will vary and V_q is adjusted to keep W constant. So, the evolution of V_q in T should be a straight line whose slope is $k\frac{h}{Nb^2}$. We have represented in figure 9 the result curves for several values of W and both rotational directions.

The results show that the experimental trials and the modelling are consistent, since the curves are nearly straight. However, the slope of these lines depends on the level of the stator's deformation W and also on the direction of rotation. These variations reveal non-linearities in the modelling; in fact, they express the limits of this modelling, and more specifically the limit imposed by the assumption that there is only one contact point. This is why, an average value of $k\frac{h}{b^2}$ is then calculated from the trials, and the slope of the curves drawn on figure 9.

So, the averaged slope of all those lines is $480NmV^{-1}$ yielding:

$$k\frac{h}{b^2} = 67.2m^{-1}$$

The value of this parameter has to be compared to the one calculated from an analytical approach. In fact, considering the geometrical dimensions of the motor under study, kh/b can be evaluated to 107m-1. The gap between these two estimated values can be first explained by the difficulty to estimate the parameter h, that characterizes the neutral plane location. Secondly, this result may be induced by the modelling assumptions, in particular, the punctual contact one. Nevertheless, the approach leads to a modelling structure that we are able to identify and which agrees with the torque characteristics in a given validity domain. n

C. Experimental tries

Different trials have been carried out to illustrate the performance of this torque estimator. The first measurements shown in figure 10 depict the evolution of the estimated load torque and the measured

CW rotational direction

CCW Rotational direction

Fig. 7. $\frac{W}{V}$ as a function of Ψ and comparison with the modelling.

TABLE I
IDENTIFIED VALUES OF THE PARAMETER d_s FOR EACH ROTATIONAL DIRECTION.

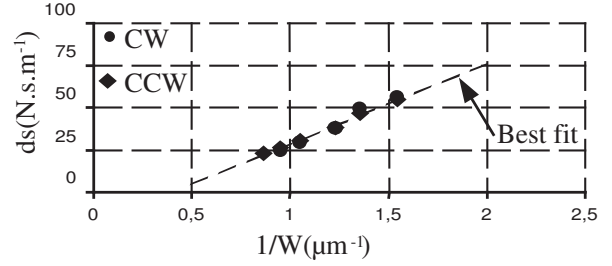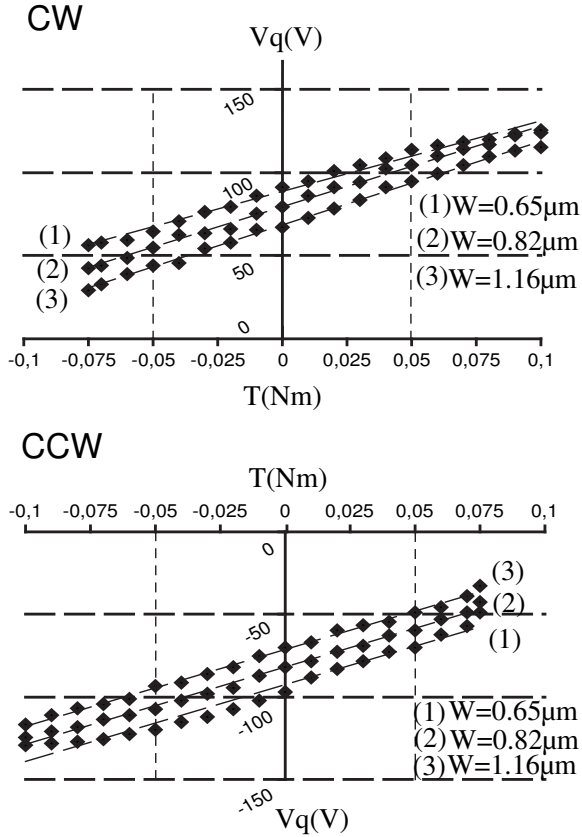| W(μm)	0.65	0.74	0.82	0.95	1.05
$d_s(N.s.m^{-1})$, CW	54.6	46.5	38.2	30.6	26.1
$d_s(N.s.m^{-1})$, CCW	56.3	49.74	38.2	29.7	24.9

this method.

It appears that d_s depends more on the operating wave amplitude W and less on the rotational direction. In order to take into account this non linearity in the torque estimator, we are led to representing in figure 8 the evolution of d_s in W, or rather in $\frac{1}{W}$ because this results in a linear shape.

Equation 28 then fits this curve:

$$d_s = -d_{s0} + \frac{\rho}{W} \qquad (28)$$

The values of d_{s0} and ρ are obtained from the figure 8:

Fig. 9. V_q as a function of T and comparison a straight line.

load torque for both rotational directions. During this trial, the stator wave's amplitude was kept constant while the load torque T was time varying.

The second measurement of figure 11 shows the evolution of the measured load torque compared to its estimation when W was time varying. Both rotational directions are depicted, though motor operation ($T > 0$ and $\omega > 0$, or $T < 0$ and $\omega < 0$) and brake operation ($T < 0$ and $\omega > 0$, or $T > 0$ and $\omega < 0$) were here experienced.

Considering that the torque estimator is quite straightforward, the estimated load torque is found to be consistent with the measurements of the experimental trials of figures 11 and 10.

Estimation errors can however be measured on figure 11, revealing that the estimation depends on W. More obviously, errors are amplified for braking operations while they are acceptable for other conditions. This is mainly due to the averaged value of $k\frac{h}{b^2}$ we had to use in equation 29 and which is a tradeoff between all the values identified for all the operating points of the chapter III-B. Performances of the estimator could then be improved by taking into account the variation of $k\frac{h}{b^2}$ in W, but this would be achieved at the expense of complexity. Despite this problem, applications can take advantage of this torque estimator, and this is dealt with in the next section.

IV. APPLICATION: LIMITING THE TIGHTENING FORCE OF TWUM ACTUATED CLAW

A. Working principle of a claw

Because of torque vs speed characteristics, Travelling Wave Ultrasonic Motors are very suitable for applications which need a low speed but a high torque. In this field of applications, the electrically actuated claws are devices which are widely used, for example at the end of a robot arm to allow object prehension.

Different controls of the claw can be achieved. The first control type is a position control of the actuator of the claw between an opened position till the closed position. This is well suited for objects which all have the same dimensions. But if variable objects of random sizes have to be picked up, the larger objects are held extremely tight, while the smallest ones are not even caught (figure 12).

This is why, instead of having a claw position control, a force limitation is preferred. In this operating mode, the claw closes up at a constant speed until the force at the claw 's tip reaches a limited value.

This last control method is quite easy to achieve with electromagnetic motors, because the torque is proportional to the supply current which is often controlled, and can thus be limited. But those motors have high speed characteristics, so they need a speed reducer in order to adapt the output speed of the shaft to the desired speed of the claw when closing. This increases the system's bulk and its cost.

In this application, a TWUM is interesting, because it can be directly mounted on the claw since its low-speed characteristic is well adapted to the system. The torque estimator developed in this article is implemented to ensure the limitation of the tightening force.
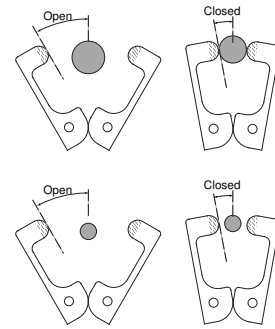

Fig. 12. Effect of a controlled position claw when the object is sufficiently big, and in the case where it is too small.

The algorithm for the closing will be as follows:

- 1 wait for the starting signal
- 2 close with a constant speed. During this step, W is kept constant, and the torque is estimated on line
- 3 stop the motor (set W to 0) when the torque estimator has reached a value previously fixed.

The next section presents the experimental runs of the claw actuated by a TWUM, with its torque limitation. from now on the limited value of the estimated torque will be referred to as T_{lim}

B. Experimental runs

The claw fixed on the TWUM's shaft is depicted in figure 13. Several objects with different sizes can be positioned, and for each run, the internal variable of the motor can be recorded. Thus, figure 14 depicts the evolution of V_q (measured with ψ), the motor rotational angle, the measured and estimated torque and finally the wave amplitude W - which is also controlled. These curves are obtained with $T_{lim} = 0.05Nm$. The cycle begins at $t = 0$ with the starting signal; a wave amplitude reference of about $1\mu m$ is ordered, and the claw closes. The estimated torque as well as the measured one are initially null, but at $t = 50ms$ they both start to increase because the claw is in contact with the object to be grasped. Consequently, V_q increases in accordance equation (29), since W is kept constant.
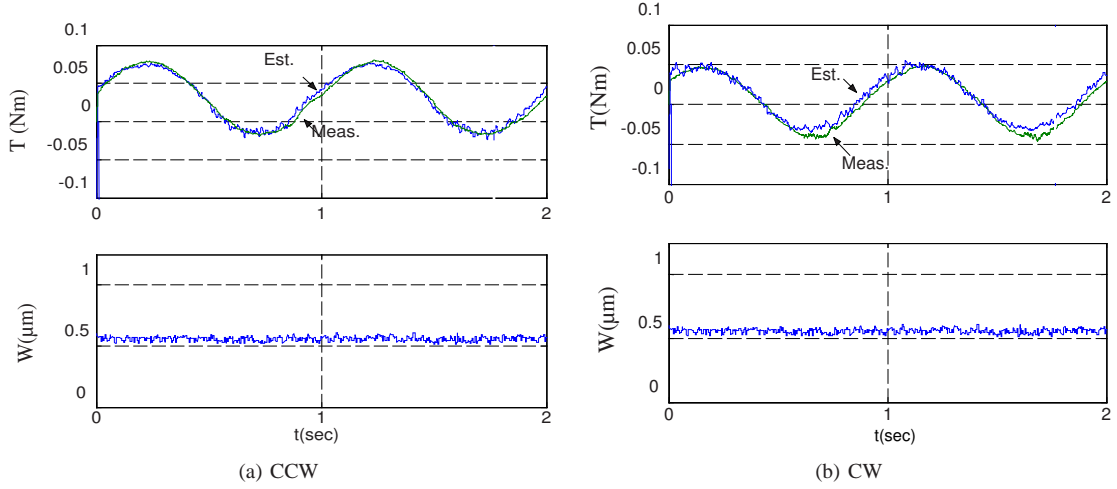
(a) CCW   (b) CW

Fig. 10. Comparison between the actual load torque and the estimator's output for a constant travelling wave's amplitude.

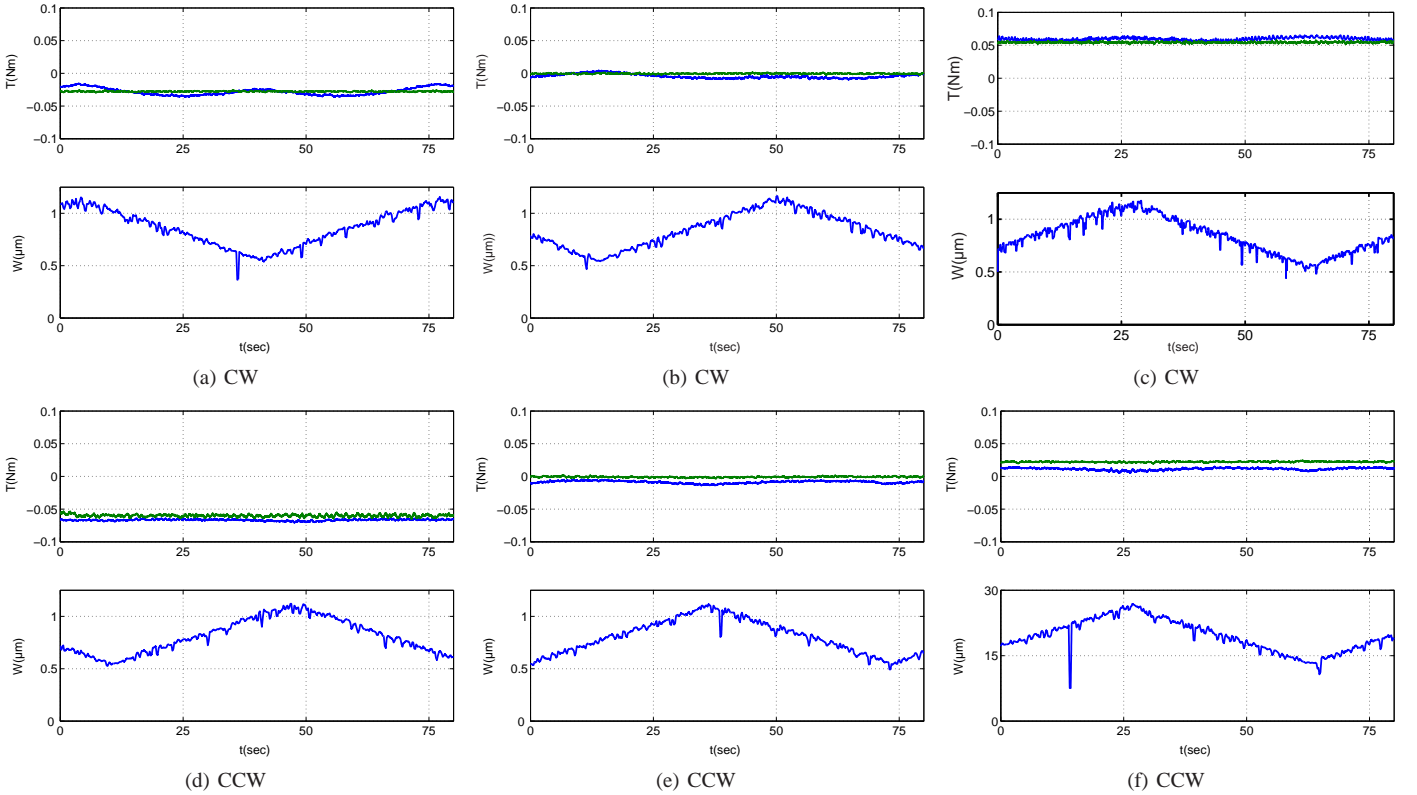(a) CW   (b) CW   (c) CW

(d) CCW   (e) CCW   (f) CCW

Fig. 11. Measurement and estimation of the load torque for a time varying wave amplitude.

At $t = 85ms$, the estimated torque reaches the limitation: a reference value of W of $0\mu m$ is ordered which is obtained in almost $10ms$. During this short time, the torque actually applied to the claw can be a little larger due to the time the wave amplitude needs to become null. Then the torque estimator is switched off because the very low wave amplitude leads to erroneous estimated torque values.

So, the claw stops its grasping action when it meets an object. This contact is detected through an increasing in the motor's torque, which is estimated on line. Of course, the force with which the object is taken depends on the value of T_{lim}. In figure 15, we have drawn the evolution of the estimated and the measured torque for several values of T_{lim}. This run shows that it is possible to limit the tightening force

of the claw by tuning the value of T_{lim}.[1]

We must emphasize here that the control presented is not a torque regulation, but a torque limitation. In fact, when the motor is stopped, the force on the claw 's tips can change due to external conditions. A torque regulation implies that the torque keeps a constant value, even at null speed, this could be achieved with an improvement of the torque estimator at low wave amplitude. However, a limitation is enough in applications in which the objects are inanimate.

---

[1]The measured torque is actually about $0.04Nm$ above the estimated one. This gap is due to the inertia of the torque sensor which creates a torque when the motor is breaking($J_t = 10^{-5}kgm^2$). Better results should be obtained for a claw directly mounted on the motor's shaft.
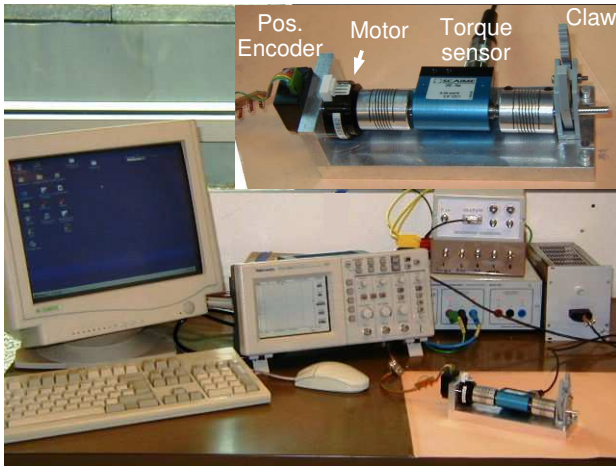
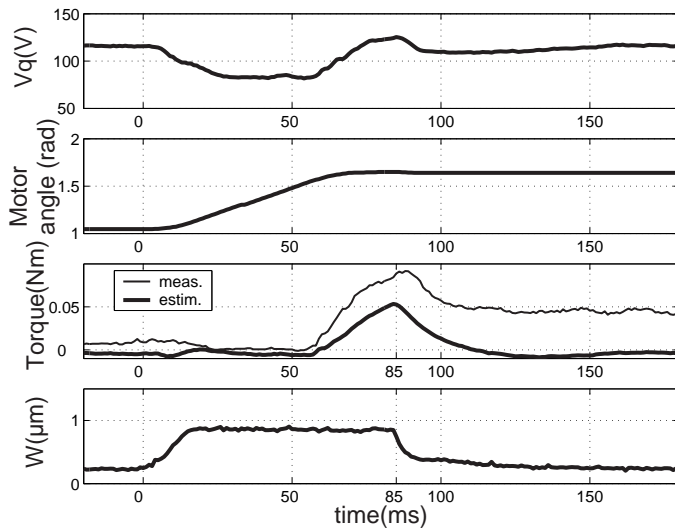Fig. 13. The experimental Setup.

Fig. 14. Internal variables of the motor for a closing sequence of a TWUM actuated claw , with limitation of the torque.
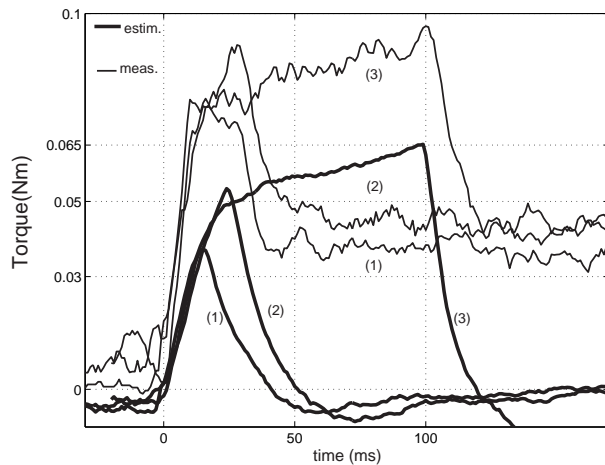

Fig. 15. Comparison of the output torque for several value of the limiting value of T: (1) $T_{lim} = 0.03Nm$, (2) $T_{lim} = 0.05Nm$, (3) $T_{lim} = 0.065Nm$.

V. CONCLUSION

In this article, we have presented a method to achieve a torque estimator for a TWUM. This estimator relies on the causal modelling of the motor which helps to deduce the estimator's equation. Compared to the torque estimators which rely on the torque/speed characteristics of the motor, we emphasize that the estimator presented here doesn't need the measurement of the rotational speed of the motor, this allows to removal of the speed sensor, and the measurements have confirmed the global structure of the modelling.

Experimental trials have been carried out to check the performances of the estimator along a wide range of operations, for time varying torque and for time varying speed of the motor. Results have been consistent with the measurements, but we highlighted that any non-linearities could reduce confidence in the estimation.

Although all the questions related to the precision of the estimated torque – especially for operations where W is varying – are still open, the estimator is tested on an application in the final section. We use a claw actuated by a TWUM. Several trials have shown that the device runs well, and we have shown that the tightening force of the claw can be tuned by adjusting the limited value of the estimated torque.

Future work should increase the precision of this torque estimator, more specifically at low rotational speeds, to allow sensorless torque regulators. This implies the control of voltages phases leading to the loss of quadrature. A new modelling should be introduced to take into account this voltage supply.

VI. ACKNOWLEDGMENT

REFERENCES

[1] J.Maas, T.Schulte, N.Fröhleke. Model based control for ultrasonic motors. *IEEE trans. on Ultrasonics, Ferroelectrics and Frequency control*, 5:165–180, june 2000.
[2] Toshiiku Sashida, Takashi Kenjo. *An introduction to Ultrasonic Motors*. Clarendon Press, 1993.
[3] F.Giraud, B.Semail, J.-T.Audren. Analysis and phase control of a piezo electric travelling wave ultrasonic motor for haptic stick application. *IEEE trans. on Industry applications*, 40:1541–1549, nov-dec 1997.
[4] F.Giraud, B.Lemaire-Semail. Causal modeling and identification of a travelling wave ultrasonic motor. *European Physical Journal of Applied Physics*, 21:151–159, february 2003.
[5] W. Hagood IV, A.J. McFarland. Modeling of a piezoelectric rotary ultrasonic motor. *IEEE Transactions on ultrasonics, ferrelectrics and frequency control*, 42(2), march 1995.
[6] J.Maas, P.Ide, N.Fröhleke, H.Grostollen. Simulation model for ultrasonic motors powered by resonant converters. *IAS'95*, 1:111–120, October 1995.
[7] H.Hirata, S.Ueha. Characteristics estimation of a travelling wave type ultrasonic motor. *IEEE trans. on Ultrasonics, Ferroelectrics and Frequency control*, 40:402–406, july 1993.
[8] T.Maeno, T.Tsukimoto, A;Miyake. Finite element analysis of the rotor/stator contact on e ring-type ultrasonic motor. *IEEE trans. on Ultrasonics, Ferroelectrics and Frequency control*, 39:668–674, july 1993.
[9] J.Maas, T. Schulte, H.Grostollen. Optimized drive control for inverter-fed ultrasonic motors. *IEEE Industry applications society (IAS'97)*, 1:690–698, 1997.
[10] ShinseI. Internet web site. *http://www.tky.3web.ne.jp/∼usrmotor/ English/html/*.
[11] N. El ghouty. *Hybrid modeling of a traveling wave piezo electric motor*. PhD thesis, Aalborg University, department of control engineering, May 2000.
[12] J.Maas, H.Grostollen. Averaged model of inverter-fed ultrasonic motors. *IEEE power electronics specialists conf. (PESC)*, 1:740–786, 1997.

Frédéric Giraud was born in France in 1973. He is graduated from Ecole Normale Supérieure de Cachan, France in 1996 and received the B.S. degree in electrical engineering from Paris-XI University, Orsay, France in 1995, the M.S. Degree in electrical engineering in 1997 from the Institut National Polytechnique de Toulouse,Toulouse, France, and the phD degree from the Lille University, in 2002. He's a member of the electrical engineering and power electronics laboratory of Lille (L2EP) as an Assistant Professeur. His research deals with the modelling and the control of standing wave and travelling wave piezo-electric actuators, for positioning and force feedback applications.

Betty Semail was born in Arras, France, on February 27, 1964. She received her Ph. D degree in 1990 from University of Paris XI, Orsay and habilitation degree in 1997 from University of science and technologies of Lille. Since 1990 she has been assistant professor in Ecole Centrale of Lille and she is now professor in university of Lille 1. She is member of the electrical engineering and power electronics laboratory of Lille (L2EP) and responsible of the research axis upon control of electrical systems. She has been working motors and her main field of interest now deals with the modelling and control of piezo-electric actuators, for positioning and force feedback applications.